Astronomy & Astrophysics manuscript no. secsnr
March 29, 2012

Secondary Cosmic Ray Nuclei from Supernova Remnants and Constraints to the Propagation Parameters

Nicola Tomassetti[1] and Fiorenza Donato[2]

[1] Perugia University and INFN, Perugia 06100 Italy
[2] Torino University and INFN, Torino 10125 Italy

March 2012

ABSTRACT

Context. The secondary-to-primary B/C ratio is widely used to study the cosmic ray (CR) propagation processes in the Galaxy. It is usually assumed that secondary nuclei such as Li-Be-B are entirely generated by collisions of heavier CR nuclei with the interstellar medium (ISM).
Aims. We study the CR propagation under a scenario where secondary nuclei can also be produced or accelerated from galactic sources. We consider the processes of hadronic interactions inside supernova remnants (SNRs) and re-acceleration of background CRs in strong shocks. We investigate their impact in the propagation parameter determination within present and future data.
Methods. Analytical calculations are carried on in the frameworks of the diffusive shock acceleration theory and the diffusive halo model of CR transport. Statistical analyses are performed to determine the propagation parameters and their uncertainty bounds using the existing data on the B/C ratio as well as the simulated data expected from the AMS-02 experiment.
Results. The spectra of Li-Be-B nuclei emitted from SNRs are harder than those due to CR collisions with the ISM. The secondary-to-primary ratios flatten significantly at $\sim$ TeV/n energies, both from spallation and re-acceleration in the sources. The two mechanisms are complementary to each other and depend on the properties of the local ISM around the expanding remnants. The secondary production in SNRs is significant for dense background media, $n_1 \gtrsim 1\,\mathrm{cm}^{-3}$, while the amount of re-accelerated CRs is relevant for SNRs expanding into rarefied media, $n_1 \lesssim 0.1\,\mathrm{cm}^{-3}$. Due to these effects, the the diffusion parameter δ may be misunderstood by a factor of $\sim$ 5–15%. Our estimations indicate that an experiment of the AMS-02 caliber can constrain the key propagation parameters while breaking the source-transport degeneracy, for a wide class of B/C-consistent models.
Conclusions. Given the precision of the data expected from on-going experiments, the SNR production/acceleration of secondary nuclei should be considered, if any, to prevent a possible mis-determination of the CR transport parameters.

Key words. cosmic rays — supernova remnants — acceleration of particles — nuclear reactions, nucleosynthesis, abundances

1. Introduction

The problems of the origin and propagation of the charged cosmic rays (CRs) in the Galaxy are among the major subjects of the modern astrophysics. It is generally accepted that *primary* CR nuclei such as H, He, C, N and O, are accelerated in supernova remnants (SNRs) via diffusive shock acceleration (DSA) mechanisms, that produce power-law momentum spectra (Drury, 1983). At relativistic energies $S \propto p^{-\nu} \sim E^{-\nu}$. After being accelerated, CRs are released in the circumstellar environment where they diffuse through the turbulent magnetic fields and interact with interstellar matter (ISM) (Strong et al., 2007). Due to diffusion, CRs stream out from the Galaxy with a characteristic time $\tau_{\rm esc} \propto E^{-\delta}$. The spectrum of primary CR nuclei predicted at Earth is therefore $N_p \sim S\,\tau_{\rm esc}$. Their nuclear collisions with interstellar gas are believed to be the mechanism producing the *secondary* CR nuclei, such as Li, Be, and B, which are underabundant in the thermal ISM. Thus, the equilibrium spectra of secondary CRs are $E^{-\delta}$ times softer than those of their progenitors. At energy above some tenths of GeV per nucleon, where CR nuclei reach the pure diffusive regime, this picture predicts power-law distributions such as $N_p \sim E^{-\nu-\delta}$ for primary nuclei and $N_s/N_p \sim E^{-\delta}$ for secondary-to-primary ratios at Earth. These trends may be straightforwardly derived from the analitical solutions in Maurin et al. (2001). Present observations indicate $\delta \sim 0.3$–0.7 and $\nu \sim 2.0$–2.4. The bulk of data is collected at $E \lesssim 10\,\mathrm{GeV\,nucleon}^{-1}$, where the CR spectra are shaped by additional effects such as diffusive reacceleration, galactic wind convection, energy losses and solar modulation. Since there is no firm theoretical prediction for the key parameters associated with these effects, it is very difficult to disentangle each physical component by the use of the experimental data. The Boron to Carbon (B/C) ratio is the best measured secondary-to-primary ratio and it is used to constrain several of the model parameters. Throughout this paper we call *secondaries* all CR nuclei resulting as products of hadronic interactions, independently on the location where they originate. The standard approach, hereafter *reference model*, assumes that the secondary nuclei are absent in the CR sources.

In this paper we examine two mechanisms that produce a source component of secondary CRs: (i) the fragmentation of CR nuclei inside SNRs and (ii) the re-acceleration by SNRs of pre-existing CR particles. The secondary CR production inside SNRs was studied in Berezhko et al. (2003) and recently reconsidered to describe the positron fraction (Blasi, 2009; Ahlers et al., 2009). Predictions for the $\bar{\rm p}/{\rm p}$ ratio (Blasi & Serpico, 2009) and for the B/C ratio (Mertsch & Sarkar, 2009) have also been investigated. An interesting aspect of this mechanism is that, if the secondary fragments start the DSA, the secondary-to-primary ratios must eventually increase. Similarly, the re-acceleration of background CRs interacting with the expanding SNR shells may in-

duce significant transformations of their spectra at high energies (Berezhko et al., 2003; Wandel et al., 1987). In particular, the re-acceleration redistributes the spectrum of secondary nuclei to a spectrum $S \sim E^{-\nu}$. The main feature of both mechanisms is that they produce hard spectra of secondary nuclei compared with their standard production from primary CR collisions on the ISM. These source components of secondary CRs may become relevant at ~ TeV energies. Thus, disregarding such effects may provoke a mis-determination of the CR transport parameters. The aim of this paper is to examine their impact in the CR propagation physics. This task requires a description of the CR acceleration processes in SNRs and their interstellar propagation. In this work we use fully analytical calculations in the frameworks of the linear DSA theory and the diffusion halo model (DHM) of CR transport. In Sect. §2 we present the DSA calculations for CR nuclei, including standard injection from the thermal ISM, hadronic interactions and re-acceleration. Sect. §3 outlines the basic elements of the DHM galactic propagation. In Sect. §4 we show our model predictions for the CR spectra and ratios at Earth; we study the impact of the secondary source components in the determination of the CR transport parameters. In Sect. §5 we present our estimates for the Alpha Magnetic Spectrometer (AMS). We conclude in Sect. §6.

2. Acceleration in SNR Shock Waves

We compute the spectrum of CR ions accelerated in SNRs using the DSA theory (Drury, 1983), including the loss and source terms the production and acceleration of secondary fragments. Our derivation is formally similar to that in Morlino (2011), but the physical problem is that dealed in Mertsch & Sarkar (2009). Within this formalism, we also compute the re-acceleration of pre-existing CR particles.

2.1. DSA Calculations

We consider the case of plane shock geometry in test-particle approximation, *i.e.*, ignoring the feedback due to the CR pressure on the shock dynamics. The shock front is in its rest-frame at $x = 0$. The un-shocked upstream plasma flows in from $x < 0$ with speed u_1 (density n_1) and the shocked downstream plasma flows out to $x > 0$ with speed u_2 (density n_2). These quantities are related by the compression ratio $r = u_1/u_2 = n_2/n_1$. The particle spectra are described by the phase space density $f(p, x)$. The equation that describes the diffusive transport and convection at the shock for a j–type nucleus (charge Z_j and mass number A_j) reads:

$$u\frac{\partial f_j}{\partial x} = D_j\frac{\partial^2 f_j}{\partial x^2} + \frac{1}{3}\frac{du}{dx}p\frac{\partial f_j}{\partial p} - \Gamma_j^{\rm inel} f_j + Q_j\,, \qquad (1)$$

where $D_j(p)$ is the diffusion coefficient near the SNR shock, u is the fluid velocity, $\Gamma_j^{\rm inel} = \beta_j c n \sigma_j^{\rm inel}$ is the total destruction rate for fragmentation (see Sect. §2.3), $\sigma_j^{\rm inel}$ is the cross section for the process, and $Q_j(x, p)$ represents the source term. Solutions of Eq. 1 can be found, separately, in the regions upstream ($x < 0$) and downstream ($x > 0$) to the shock front, by requiring $\partial f/\partial x = 0$ for $x \to \mp\infty$. We drop the label j characterizing the nuclear species, and make use of the subscript $i = 1$ ($i = 2$) to indicate the quantities in the upstream (downstream) region. We define the quantities:

$$\lambda_i = \frac{u_i}{D_i}(\Lambda_i - 1) \qquad \kappa_i = \frac{u_i}{D_i}(\Lambda_i + 1)\,, \qquad (2)$$

where we have denoted $\Lambda_i = \sqrt{1 + 4D_i\Gamma_i^{\rm inel}/u_i^2}$. The solution can be expressed in the following form:

$$f(x,p) = \begin{cases} f_0(p)e^{-\frac{1}{2}\kappa_1 x} - \frac{U_1+V_1+W_1}{u_1\Lambda_1} & (x<0) \\ \\ f_0(p)e^{+\frac{1}{2}\lambda_2 x} + \frac{U_2+V_2+W_2}{u_2\Lambda_2} & (x>0) \end{cases} \qquad (3)$$

where the downstream integral terms U_2, V_2 and W_2 are given by:

$$\begin{aligned} U_2(x,p) &= +\int_x^{+\infty} Q_2(x',p)e^{\frac{1}{2}\kappa_2(x-x')}dx' \\ V_2(x,p) &= +\int_0^{x} Q_2(x',p)e^{-\frac{1}{2}\lambda_2(x-x')}dx' \\ W_2(x,p) &= -\int_0^{+\infty} Q_2(x',p)e^{-\frac{1}{2}(\lambda_2 x+\kappa_2 x')}dx' \end{aligned} \qquad (4)$$

In the upstream region, U_1, V_1 and W_1 are still given by Eq. 4 after performing the substitutions: $1 \to 2$, $\kappa_2 \to -\lambda_1$, $\lambda_2 \to -\kappa_1$, and $\infty \to -\infty$. The distribution function at the shock position, f_0, is determined by the matching conditions at $x = 0$. We integrate Eq. 1 in a thin region across the shock front. Assuming that $D \equiv D_1 = D_2$, we find the equation for f_0:

$$p\frac{\partial f_0}{\partial p} = -\alpha f_0(p) - \alpha j(p) + \frac{\alpha}{u_1}G(p)\,, \qquad (5)$$

where $\alpha = 3u_1/(u_1 - u_2)$ is the known DSA spectral index. The term G denotes the sum of the upstream and downstream source integrals:

$$G(p) = \int_{-\infty}^{0} Q_1 e^{\frac{1}{2}\lambda_1 x'}dx' + \int_0^{\infty} Q_2 e^{-\frac{1}{2}\kappa_2 x'}dx' \qquad (6)$$

The function $j(p)$ is linked to the destruction term $\Gamma^{\rm inel}$. It is defined as:

$$j(p) = \frac{1}{2}(\Lambda_1 - 1) + \frac{1}{2r}(\Lambda_2 - 1) \qquad (7)$$

After defining the function:

$$\chi(p,p') = \alpha\int_{p'}^{p}\frac{j(p'')}{p''}dp''\,, \qquad (8)$$

the solution of Eq. 5 can be expressed in the simple form:

$$f_0(p) = \alpha\int_0^p \left(\frac{p'}{p}\right)^{\alpha}\frac{G(p')}{u_1}e^{-\chi(p,p')}\frac{dp'}{p'} \qquad (9)$$

From Eq. 3 one recovers the standard DSA solution setting $\Gamma^{\rm inel} = 0$ (no interactions) and assuming that the injection occurs only at the shock front ($U_i = V_i = W_i = 0$): one finds $f_2 = f_0$ and $f_1 = f_0 e^{u_1 x/D_1}$, while Eq. 9 gives a spectrum $p^{-\alpha}$, provided that the source term $G(p)$ is softer than $p^{-\alpha}$ (see Sect. §2.4). Some simplifications can be made by analyzing the time-scales of the problem. The DSA acceleration rate for particles of momentum p in a stationary shock is $\Gamma^{\rm acc} \sim \frac{u_1^2}{20\,D}$, where we assumed Bohm diffusion ($D \propto p$) and strong shocks ($r \approx 4$). For a SNR of age $\tau_{\rm snr}$, the condition $\Gamma^{\rm acc} \equiv \tau_{\rm snr}^{-1}$ defines the maximum momentum $p^{\rm max}$ attainable by DSA. In the presence of hadronic interactions, the requirement $\Gamma^{\rm inel} \ll \Gamma^{\rm acc}$ must be fulfilled. These relations imply $20\,\Gamma^{\rm inel}D/u^2 \ll 1$ and $x\Gamma^{\rm inel}/u \ll 1$ at all the energies considered. Under such conditions, we can linearly expand $\Lambda \approx 1 + 2\Gamma^{\rm inel}D/u^2$, so that $\lambda \approx 2\Gamma^{\rm inel}/u$ and $\kappa \approx 2u/D + 2\Gamma^{\rm inel}/u$. The exponential terms of Eq. 3, Eq. 4 can also be expanded as

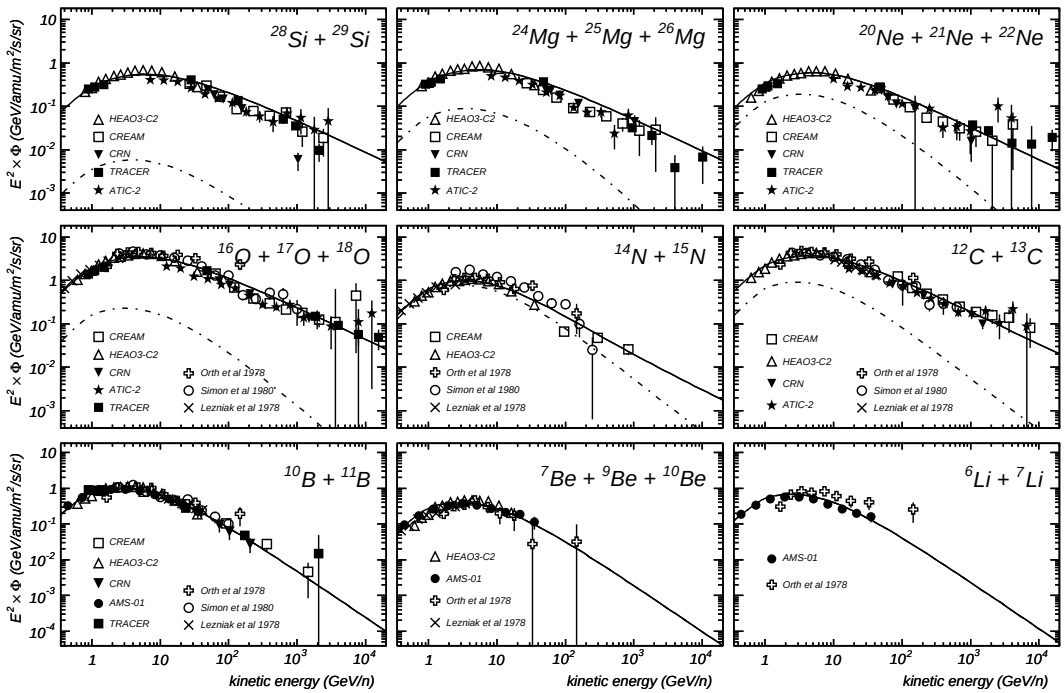

Fig. 1. Energy spectra of the CR elements Li, Be, B, C, N, O, Ne, Mg and Si. The solid lines represent the *reference model* prediction. The dashed lines indicate the secondary CR component arising by collisions in the ISM of the heavier nuclei. The model parameters are listed in Table 1. Data are from HEAO3-C2 (Engelmann et al., 1990), CREAM (Ahn et al., 2009), AMS-01 (Aguilar et al., 2010), TRACER (Ave et al., 2008; Obermeier et al., 2011), ATIC-2 (Panov et al., 2009), CRN (Müller et al., 1991), Simon et al. (1980), Lezniak & Webber (1978) and Orth et al. (1978). The Li-Be-B data from CREAM and AMS-01 are combined with our model to obtain the spectra from their secondary-to-primary ratios.

$e^{\frac{1}{2}\lambda x} \approx 1 - \frac{\Gamma_1^{\rm inel}}{u}x$ and $e^{\frac{1}{2}\kappa x} \approx e^{u/D}\left(1 + \frac{\Gamma_1^{\rm inel}}{u}x\right)$. Thus, the function $j(p)$ of Eq. 7 reads:

$$j(p) \approx \alpha(1+r^2)\frac{\Gamma_1^{\rm inel} D(p)}{u_1^2}\,, \qquad (10)$$

and the integral of Eq. 8 leads to:

$$\chi(p,p') \approx \alpha(1+r^2)\frac{\Gamma_1^{\rm inel}}{u_1^2}[D(p) - D(p')]\,, \qquad (11)$$

that recovers Mertsch & Sarkar (2009). Below we show the DSA solutions for primary nuclei (injected at the shock), their secondary fragments (generated in the SNR environment) and for pre-existing CR particles that undergo re-acceleration.

2.2. Acceleration of Primary Nuclei

The injection of ambient particles is assumed to occur immediately upstream the shock at momentum $p^{\rm inj}$. The source term for primary nuclei reads:

$$Q^{\rm pri}(x,p) = Y\,\delta(x)\,\delta(p - p^{\rm inj})\,. \qquad (12)$$

Particles can be injected only when their *Larmor radius* is large enough to cross the shock thickness. Thus, we assume a reference injection rigidity for all nuclei, $R^{\rm inj}$, so that $p^{\rm inj} = ZR^{\rm inj}$. The constants Y_j reflects the particle abundances in the ISM and their injection efficiencies. In this work, they are determined by the data. The phase space density profile is given by:

$$f(x,p) \approx \begin{cases} f_0(p) e^{u_1 x/D(p)} & (x<0)\,, \\ f_0(p)\left(1 - \frac{\Gamma_2^{\rm inel}}{u_2}x\right) & (x>0) \end{cases} \qquad (13)$$

The upstream profile, $\sim e^{u_1 x/D}$, indicates that the plasma is confined near the shock within a typical distance $\sim D/u_1$. Due to advection, the particles are accumulated in the downstream region, where destruction processes give rise to the term $\frac{\Gamma_2^{\rm inel}}{u_2}x$. The momentum spectrum at the shock position is $f_0 \propto e^{-\chi} p^{-\alpha}$, which is the known DSA power-law behaviour times an exponential factor, $\sim e^{-\chi}$, given by $\chi \approx \alpha\Gamma^{\rm inel}/\Gamma^{\rm acc}$. The condition $\Gamma^{\rm acc} \ll \tau_{\rm snr}^{-1}$ implies $\chi \lesssim 1$.

2.3. Production and Acceleration of Secondary Nuclei

Secondary nuclei originate in the SNR environment from spallation of heavier nuclei on the background medium. The source term for a j-type CR species arises from the sum of all heavier k-type nuclei, $Q_j^{\rm sec} = \sum_{k>j} Q_{kj}^{\rm frag}$. Each partial contribution reads:

$$Q_{kj}^{\rm frag}(x,p) = \frac{1}{4\pi p^2}\int_{p^{\rm inj}}^{\infty} N_k(x,p')\Gamma_{kj}^{\rm frag}(p')\delta(p - \xi_{kj}p')dp'\,, \qquad (14)$$

where $N_k(x,p') = 4\pi p'^2 f_k(x,p')$ is the progenitor number density and $\Gamma_{kj}^{\rm frag} = \beta_k c n \sigma_{kj}^{\rm frag}$ is the $k \to j$ fragmentation rate, which is implicitly summed over the circumstellar abundances (Hydrogen and Helium components). We have assumed that the kinetic energy per nucleon is conserved in the process, *i.e.*, the fragments are ejected with momentum $\xi_{kj} = A_j/A_k$ times smaller than that of their parents. The presence of short-lived isotopes (*ghost nuclei*) such as ^{9}Li or ^{11}C is reabsorbed in the definition of σ_{kj}, while long-lived isotopes such as ^{10}Be or ^{26}Al (lifetime ~ 1 Myr) are considered as stable during the acceleration process (time-scale $\tau_{\rm snr} \sim 10$ kyr). The source spatial profile takes the form of the progenitor nucleus of Eq. 13. In the upstream

region, one has $Q_{jk}^{\rm frag} = q_{1,kj} e^{u_1 x/D_k}$, where D_k is the diffusion coefficient of the progenitor nucleus at the momentum p/ξ_{kj}. For $D \propto p/Z$, one can write $D_k(p/\xi_{kj}) = \zeta_{kj} D_j(p)$, where $\zeta_{kj} = \frac{A_j Z_k}{A_k Z_j}$. In practice $\zeta_{kj} \approx 1$ for all processes $k \to j$ with $Z_{j,k} > 2$. The terms at the shock, $q_{1,jk}$ and $q_{2,jk}$, are given by:

$$q_{i,kj}(p) = \xi_{kj}^{-3} f_{0,k}(p/\xi_{kj}) \Gamma_{i,kj}^{\rm frag}\,, \tag{15}$$

and the downstream solution reads:

$$f_{2,j}(x,p) = f_{0,j}(p) + \left[\frac{q_{2,j}(p)}{u_2} - \Gamma_{2,j}^{\rm frag} f_{0,j}(p)\right] x\,, \tag{16}$$

where $f_{0,j}$ is given from Eq. 9 using $G(p)$ by the following expression:

$$G_{kj}(p) = q_{1,kj}(p) \frac{D_j(p)}{u_1} \left(\zeta_{kj}^{-1} + r^2\right) \tag{17}$$

We solve all equations starting from the heaviest element and proceeding downward in mass. We are interested in the total contribution of SNRs to the galactic CR population. We take it as the integral of the downstream solution over the SNRs volume left behind the shock:

$$S_j^{\rm dsa}(p) = 4\pi p^2 \mathcal{R}_{\rm snr} \int_0^{x_{\rm max}} 4\pi x^2 f_{2,j}(x,p) dx\,, \tag{18}$$

where $x_{\rm max} = u_2 \tau_{\rm snr}$ and $\mathcal{R}_{\rm snr}$ is the supernovae explosion rate per unit volume in the Galaxy.

2.4. Re-Acceleration of Background CR Nuclei

Together with the thermal ISM particles of Sect. §2.2, SNR shock waves may also accelerate the background CRs at equilibrium (Berezhko et al., 2003; Wandel et al., 1987). We refer to this mechanism as *re-acceleration* of CRs in SNRs. For a prescribed distribution function of background CRs, $f_j^{\rm bg}(p)$, the DSA solution at the shock is simply:

$$f_{0,j}^{\rm re}(p) = \alpha \int_{p_j^{\rm inj}}^{p} \left(\frac{p'}{p}\right)^{\alpha} f_j^{\rm bg}(p') \frac{dp'}{p'} \tag{19}$$

Assuming, for illustrative purpose, a power-law form $f_j^{\rm bg}(p) = Y_j (p/p_j^{\rm inj})^{-s}$, the resulting re-acceleration spectrum is:

$$f_{0,j}^{\rm re}(p) = \frac{\alpha}{\alpha - s} \left[1 - (p/p_j^{\rm inj})^{-\alpha+s}\right] f_j^{\rm bg}(p) \tag{20}$$

Since the CR equilibrium spectrum, $f^{\rm bg} \propto p^{-s}$, is softer than the test-particle one ($s > \alpha$), for $p \gg p_j^{\rm inj}$ one obtains:

$$f_{0,j}^{\rm re}(p) \approx \frac{\alpha}{s - \alpha} Y_j \left(p/p_j^{\rm inj}\right)^{-\alpha} \tag{21}$$

That is, the effect of re-acceleration is to re-distribute the CR spectrum to $p^{-\alpha}$. Interestingly, in the opposite case ($s < \alpha$) the re-accelerated spectrum maintains its spectral shape p^{-s}, while its normalization is amplified by the factor $\alpha/(s-\alpha)$. In our model, however, the background spectrum $f^{\rm bg}$ is computed as discussed in Sect. §3 and takes the SNR spectra as input. Therefore, Eq. 19 is an integro-differential equation where the DSA-mechanism is fed by its DHM-propagated solution and vice-versa. On the other hand, the bulk of re-accelerated CRs comes from the low-energy part of the spectrum (below ~ 10 GV of rigidity), where the equilibrium CR spectra are fixed by the observations so they cannot vary so much. It can be safely assumed that re-accelerated CRs are a sub-dominant component of the total (integral) flux. Hence, we proceed using an iterative method as outlined in Sect. §4.5.

3. Interstellar Propagation

We use a DHM to describe the CR transport and interactions in the ISM in a 2D geometry. We disregard the effects of energy losses, diffusive reacceleration and convection. The Galaxy is modeled as a disc of half-thickness h, containing the gas and the CR sources. The disc is surrounded by a cylindrical diffusive halo of half-thickness L, radius $r_{\rm max}$ and zero matter density. CRs diffuse into both the disc and the halo. The diffusion coefficient is taken to be rigidity dependent and position independent: $K(R) = \beta K_0 (R/R_0)^{\delta}$. The number density N_j of the nucleus j is a function of the kinetic energy per nucleon, E, and the 2D position (r,z). The steady-state transport equation can be written as:

$$\left(\mathcal{W}_j^{\rm tot} - K_j \nabla^2\right) N_j = \mathcal{S}_j^{\rm tot} \tag{22}$$

The loss term, $\mathcal{W}_j^{\rm tot}$, describes the decay rate of unstable nuclei, $\tilde{\Gamma}_j^{\rm rad} = 1/(\gamma_L \tau_j)$ (γ_L is the usual Lorentz factor) and the total destruction rate for collisions in the disc, $2h\delta(z)\tilde{\Gamma}_j^{\rm inel}$. The source term, $\mathcal{S}_j^{\rm tot}$, is the sum of contributions from SNRs (the DSA solution of Eq. 18), and secondary production in the ISM from k-type progenitors:

$$\mathcal{S}_j^{\rm snr} = 2h\delta(z) s(r) S_j^{\rm dsa}(E)\,, \tag{23}$$

$$\mathcal{S}_j^{\rm ism} = 2h\delta(z) \sum_{k>j} \left(\tilde{\Gamma}_{kj}^{\rm frag} + \tilde{\Gamma}_{kj}^{\rm rad}\right) N_k\,. \tag{24}$$

The function $s(r)$ expresses the SNR radial distribution in the disc, that we take as uniform. For primary CRs, $S^{\rm dsa}$ is normalized by the Y constants of Eq. 12. In our study, secondary nuclei may have a nonzero $S^{\rm dsa}$ term. The term $\tilde{\Gamma}_{kj}^{\rm rad} = (\gamma_L \tau_{kj})^{-1}$ describe the contributions $k \to j$ from unstable progenitors of lifetime τ_{kj}. In Eq. 24 $\tilde{\Gamma}_j^{\rm inel} = \beta_j c n_{\rm ism} \sigma_j^{\rm inel}$ and $\tilde{\Gamma}_{kj}^{\rm frag} = \beta_j c n_{\rm ism} \sigma_{kj}^{\rm frag}$. The conditions $N_j \equiv 0$ at the halo boundaries and the continuity condition across the disc completely characterize the solution of Eq. 22. The full solution is reported in Maurin et al. (2001). Again, we solve the transport equations for all the CR nuclei following their top–down fragmentation sequence, plus a second iteration to account for the $^{10}{\rm Be} \to {}^{10}{\rm B}$ decay. The differential fluxes as a function of kinetic energy per nucleon E are obtained from:

$$\phi_j(E) \equiv \frac{dN_j}{d\Sigma d\Omega dt dE} = \frac{\beta c}{4\pi} N_j(E, r_\odot, 0), \tag{25}$$

where the equilibrium solutions are computed at the solar system position $(r,z) = (8.5\,{\rm kpc}, 0)$. The basic DHM predictions can be seen, for illustrative purpose, in the 1D limit $r_{max} \to \infty$. The solution for a pure primary CR reads:

$$N_p \approx \frac{S^{\rm dsa}}{K/L + \tilde{\Gamma}_p^{\rm inel}} \sim \frac{S^{\rm dsa}}{K/L}\,, \tag{26}$$

where the spallation rate is neglected for simplicity. It is apparent the effect of the propagation in steepening the spectrum: for a source spectrum $S^{\rm dsa}(E) \propto E^{-\nu}$ and a galactic diffusion coefficient of the type $K(E) \propto E^{\delta}$, the model predicts $N(E) \propto E^{-\nu-\delta}$. To resolve the two parameters ν and δ, one has to consider pure secondary species. The solution for a one-progenitor secondary CR reads as Eq. 26, with the replacement of $S^{\rm dsa}$ with $S^{\rm ism} = \tilde{\Gamma}_{sp}^{\rm frag} N_p$, so that the ratio $N_s/N_p \propto L/K$ allows the simultaneous determination of δ and K_0/L. These simple trends are valid for the *reference model*, *i.e.* when only primary CRs have source term. In the case of a secondary SNR component, depending on its intensities, the parameter determination may be more complicated.

4. Analysis and Results

Below we provide a review of the model parameters and test the *reference model* setup. Then we analyze the secondary CR production and re-acceleration in SNRs under some simple scenarios.

4.1. Model Parameters

The DSA mechanism of Sect. §2 provides power-law spectra $S^{\rm dsa} \propto E^{-\nu}$ with a unique spectral index $\nu = \alpha - 2$ for all the primary CRs, where α, in turn, is linked to the compression ratio r which is specified by δ and by the observed log-slope γ. To match $\gamma \approx 2.7$ with $\delta < 0.7$, one has to adopt a compression factor of $r < 4$ in contrast to the value $r = 4$ required for strong shocks. Despite this tension between DSA and observations, we regard r as an effective quantity describing the compression ratio actually felt by the particles, which is not necessary related to the physical strength of the SNR shocks (Ptuskin et al., 2010). The diffusion coefficient around the shock is taken to be Bohm-like, $D = \frac{pc}{3ZB}$. The ambient magnetic field B may reach $\sim 100\,\mu$G or more due to amplification effects, except in the very late SNR evolutionary stages, where the magnetic field may be damped ($B \lesssim \mu$G). In our steady-state description, the SNR parameters have to be considered as effective time-averaged quantities representing a more complex situation where the shock structure evolves with time and may be influenced by the back-reaction of accelerated CRs. The average shock speed u_1 is of the order of 10^8 cm s^{-1}. The upstream gas density, n_1, is poorly known and may well vary from $\sim 10^{-3}$ to ~ 10 cm^{-3}, depending on the SNR progenitor star or its local environment. The SNR explosion rate per unit volume is expressed as a surface density, $2h\mathcal{R}_{\rm snr}$, that we fix to 25 Myr^{-1} kpc^{-2} (Grenier, 2000).

The parameters describing the interstellar diffusion coefficient are fixed to $\delta = 0.5$ and $K_0 = 0.089$ kpc^2 Myr^{-1} (see Sect §4.2). Below the reference rigidity, $R_0 = 4$ GV, we set $\delta = 0$. However our analysis is always applied to rigidities $R > R_0$. The halo radius is $r_{\rm max} = 20$ kpc and its half-height is $L = 5$ kpc. As per the propagation in the ISM, the quantity that enters the model is surface density $h \times n_{\rm ism}$, where we take $h = 0.1$ kpc and $n_{\rm ism} = 1$ cm^{-3}. We assume a composition of 90% H + 10% He for the ISM gas density, $n_{\rm ism}$, and we assume that this composition, on average, is found in the SNR background media too. We also include the solar modulation effect though it is relevant only below few GeV nucleon^{-1}. The modulation is described in the force-field approximation (Gleeson & Axford, 1968) by means of the parameter ϕ, taken to be 500 MV, to characterize a medium-level modulation strength. Our nuclear chain starts with $Z_{\rm max} = 14$ and processes all the relevant isotopes down to $Z = 3$. Nuclei with $Z > 14$ do not contribute significantly to the Li-Be-B abundances. The spallation cross sections are taken from Silberberg et al. (1998). Cross sections on He targets are obtained by means of the algorithm presented in Ferrando et al. (1998).
The reference model parameters are listed in Table 1.

4.2. Reference Model

Before analyzing the impact of SNR production and re-acceleration of secondary CRs on the parameter determination, we test the *reference model* predictions for the parameters in Table 1. Predictions at Earth for the CR elemental spectra Li, Be, B, C, N, O, Ne, Mg and Si are presented in Fig. 1, where the total spectra (solid lines) are shown together their secondary component (dashed lines) arising by collisions in the ISM. The key quantities for propagation, K_0 and δ, are determined from the B/C ratio above 2 GeV nucleon^{-1}, using all the data reported in the last two decades, *i.e.*, by the space based experiments HEAO3-C2 (Engelmann et al., 1990), CRN (Swordy et al., 1990) and AMS-01 (Aguilar et al., 2010), and by balloon borne projects CREAM (Ahn et al., 2009) and ATIC-2 (Panov et al., 2007). The primary nuclei spectra have been normalizes using data from CREAM (for C, N, O, Ne, Mg and Si) and HEAO3-C2 (for all elements). Given the $K_0 - L$ degeneracy (see Sect. §3), in the following we will adopt the quantity K_0/L as the physical parameter, where the halo height L is fixed at 5 kpc.
As apparent from the figure, the *reference model* calculations give a good description of the CR elemental spectra within the precision of the present data. It should be noted that, under this pure diffusion model, the B/C data between ~ 10 GeV and ~ 1 TeV per nucleon suggest $\delta \sim 0.4$, while the data at lower energies ($\sim$ 1–100 GeV nucleon^{-1}) favors higher values ($\delta \sim 0.6$). These uncertainties are related on both the model unknowns at $\sim$ GeV/n energies and the lack of data at $\gtrsim 100$ GeV nucleon^{-1} (Maurin et al., 2010). We also note that the *reference model* predictions are insensitive to the source parameters n_1, u_1 and B: the source spectra are specified only by the effective compression ratio r (via γ and δ) and by the abundance constants Y. This setup is equivalent to that of many diffusion models, *e.g.* Maurin et al. (2001), that make use of rigidity power-law parameterizations as source functions.

Table 1. Source and transport parameter sets.

Acceleration Parameters		Propagation Parameters	
u_1	10^8 cm s^{-1}	K_0	0.089 kpc^2 Myr^{-1}
B	50.0 μG	δ	0.50
γ	2.7	R_0	4 GV
n_1	1 cm^{-3}	L	5 kpc
$Z_{\rm max}$	14	$r_{\rm max}$	20 kpc
$\tau_{\rm snr}$	20 kyr	h	0.1 kpc
$\mathcal{R}_{\rm snr}$	125 Myr^{-1} kpc^{-2}	$n_{\rm ism}$	1 cm^{-3}
$R_{\rm inj}$	1 GV	ϕ	0.5 GV

4.3. SNR Models

Similarly to Morlino (2011), we consider two ideal situations represented by type I/a (important for fragmentation, Sect. §4.4) and core-collapse supernovae (important for re-acceleration, Sect. §4.5). In the type I/a scenario, the supernova explodes in the regular ISM with typical density and temperature $n_1 \approx 1$ cm^{-3} and $T_0 = 10^4$ K. In the core-collapse scenario, the SNR expands into a hot diluted bubble ($n_1 \ll 1$ cm^{-3} and $T_0 \gg 10^4$ K) that may be generated either by the progenitor's wind or by precedent SNR explosions occurred in the same region. In both scenarios the circumstellar densities are assumed as homogeneous and constant during the SNR evolution. Two SNR evolutionary stages are relevant for our study: the ejecta dominated (ED) phase, when the shock front expands freely and accumulates the swept-up mass in the SNR interior, and the Sedov-Taylor (ST) expansion phase, which is driven by the thermal pressure of the hot gas. The phase transition ED–ST occurs at the time $\tau_{\rm st}$, when the swept-up mass equals the mass of the ejecta $M_{\rm ej}$. The CR acceleration ceases at the time $\tau_{\rm snr}$.

For all the models we assume $E_{\rm snr} = 5 \cdot 10^{51}$ erg, $M_{\rm ej} = 4 M_\odot$ and $\tau_{\rm snr} = 20$ kyr, where $E_{\rm snr}$ is the SNR explosion energy (not

Table 2. Case studies of type I/a and core-collapse SNRs.

SNR Model		n_1 (cm^{-3})	τ_{st} (yr)	$\bar{u_1}$ (cm s^{-1})
type I/a	I/a #1	0.5	330	1.3×10^8
	I/a #2	1.5	230	1.0×10^8
	I/a #3	3.0	183	8.9×10^7
core collapse	CC #1	0.003	1829	3.5×10^8
	CC #2	0.01	1225	2.8×10^8
	CC #3	0.1	568	1.8×10^8

converted in neutrinos) and $M_\odot$ is the solar mass. The case of different τ_{snr} values is considered in Sect. §4.6. During the ED stage the SNR radius grows with a constant rate $R_{sh}(t) = u_1 t$, at the speed $u_1 = \left(2E_{snr}/M_{ej}\right)^{1/2} \sim 10^8\,\mathrm{cm\,s^{-1}}$, until it reaches the *swept-up radius* $R_{sw} \equiv R_{sh}(\tau_{st})$. For a given SNR model characterized by n_1 and τ_{snr}, we parametrize the shock evolution (R_{sh} and u_1) using the self-similar solutions derived in Truelove & McKee (1999) for a remnant expanding into a homogeneous medium. These solutions connect smoothly the ED phase ($R_{sh} \propto t$) with the ST stage ($R_{sh} \propto t^{2/5}$). The CR acceleration ceases at the time τ_{snr}, from which we compute the average velocity $\bar{u_1} \equiv R_{sh}(\tau_{snr})/\tau_{snr}$. Thus, we use $\bar{u_1}$ as input parameter for our steady-state DSA calculations (Sect. §2.1) to compute the spectra for all the CR elements. The considered SNR models are listed in Table 2.

We always assume that the total CR flux is produced by SNRs of one type only: for each SNR model, the parameters employed have to be regarded as effective ones representing the averaged population of CR sources. Note that this simplified breakdown is somewhat artificial, because the total CR flux may be due to a complex ensemble of contributing SNRs.

4.4. Secondary CR Production in Type I/a SNRs

The secondary production is relevant for SNRs that expand into ambient densities of the order of $n_1 \sim 1\,\mathrm{cm^{-3}}$, where the quantity n_1 represents the average SNR background density. Such a value may be larger than that of the average ISM, due to, *e.g.*, contributions from SNRs located in high density regions of the galactic bulge, inside the dense cores of molecular clouds or those expanding into the winds of their progenitors.

From Eq. 16, one sees that the secondary CR flux emitted by SNRs has two components. By analogy with Blasi & Serpico (2009) and Kachelrieß et al. (2011), these are referred to as $\mathcal{A}$ and $\mathcal{B}$. The $\mathcal{A}$–term, proportional to f_0, describes the particles that are produced within a distance $\sim D/u$ from both the sides of the shock front and are still able to undergo DSA. From Eq. 17, the $\mathcal{A}$–spectrum is $f \sim p^{-\alpha+1}$, reflecting the spectrum of their progenitors ($f \sim p^{-\alpha}$) and the momentum dependence of the diffusion coefficient, $D \propto p$. The $\mathcal{B}$–term, $f \sim q_2$, describes those secondary nuclei that, after being produced, are simply advected downstream without experiencing further acceleration. Their spectrum maintains the same behaviour of that of their progenitors $q_2 \sim p^{-\alpha}$. These components are illustrated in Fig. 2 for the spectra at Earth of Li, Be and B for a SNR with $n_1 = 2\,\mathrm{cm^{-3}}$, $u_1 = 5\cdot10^7\,\mathrm{cm\,s^{-1}}$ and $B = 0.1\,\mu$G. The figure compares the standard ISM components (solid lines) with the source components $\mathcal{A}$ (short-dashed lines) and $\mathcal{B}$ (long-dashed lines) within the same propagation parameter set. Both the source components are harder than those expected from the standard CR production in ISM; in particular the $\mathcal{A}$–term leads to increasing secondary-to-primary ratios at high energies (Blasi, 2009; Mertsch & Sarkar, 2009). While the $\mathcal{B}$–term depends on the SNR ambient density n_1 and its age τ_{snr}, the $\mathcal{A}$–term also relies on the diffusion properties, as its strength is proportional to $\sim \Gamma^{frag}_{kj} D/u_1^2$. However, the parameter combination $n_1/(Bu_1^2)$ required for having a $\mathcal{A}$–term dominance at ~ TeV energies can be realized only in the latest evolutionary stage of a SNR, that is characterized by damped magnetic fields ($B \ll 1\,\mu$G) and low shock speeds ($u_1 < 10^8\,\mathrm{cm\,s^{-1}}$). On the other hand, the local flux of stable CR nuclei depends on the large-scale structure of the galaxy (some kpc) and reflects the contribution of a relatively large population of SNRs and their histories (Taillet & Maurin, 2003). Furthermore, from Eq. 9 and Eq. 11, the $\mathcal{A}$–term induces an exponential cut-off at momentum p^{cut}, given by $\chi(p^{cut}) \approx 1$, which is not observed in present data of primary or secondary CR spectra. Since our aim is to estimate these effects in the scenario where the considered SNRs produce the whole observed CRs flux, the associated parameters have to be able to accelerate all CR nuclei up to, say, $p^{max}/Z \sim 10^6\,$GV. Thus, from the requirement $\chi \lesssim 1$ for any p up to p^{max} (see Sect. §2.1), the $\mathcal{A}$-term is always ineffective at the energies we consider and will be not discussed in the following. Given the absence of a clear spectral feature in the $\mathcal{B}$–term, the spectral deformation induced by interactions in SNRs may be challenging to be detected at ~ TeV energies, because it can be easily mimicked by a different choice of δ and K_0/L. This is illustrated in Fig. 3. The total Boron spectrum (solid line) is plotted showing its standard

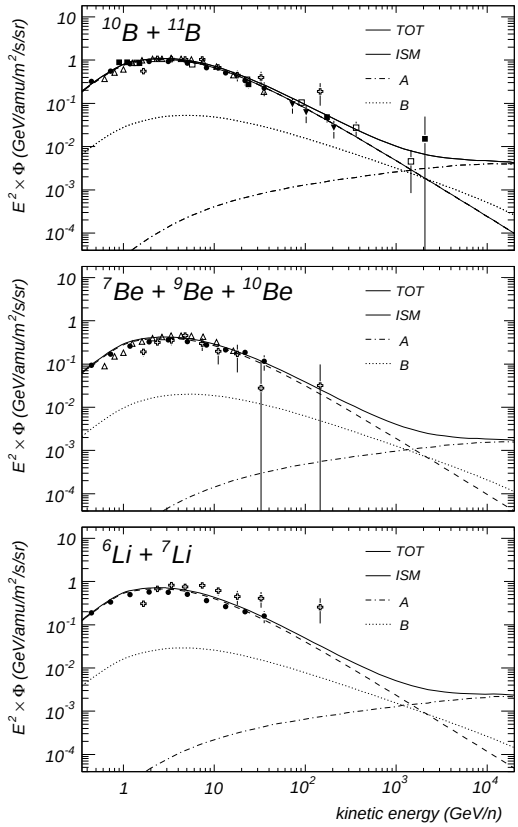

Fig. 2. Energy spectra of secondary elements Li, Be and B. The source components from fragmentation occurring inside SNRs are split into the $\mathcal{A}$-term (dot-dashed lines) and $\mathcal{B}$-term (dotted lines). The dashed lines indicate the ISM-induced components. The solid lines represent the total spectra. Source parameters are reported in the text. The propagation parameters are as in Table 1. Data as in Fig. 1.

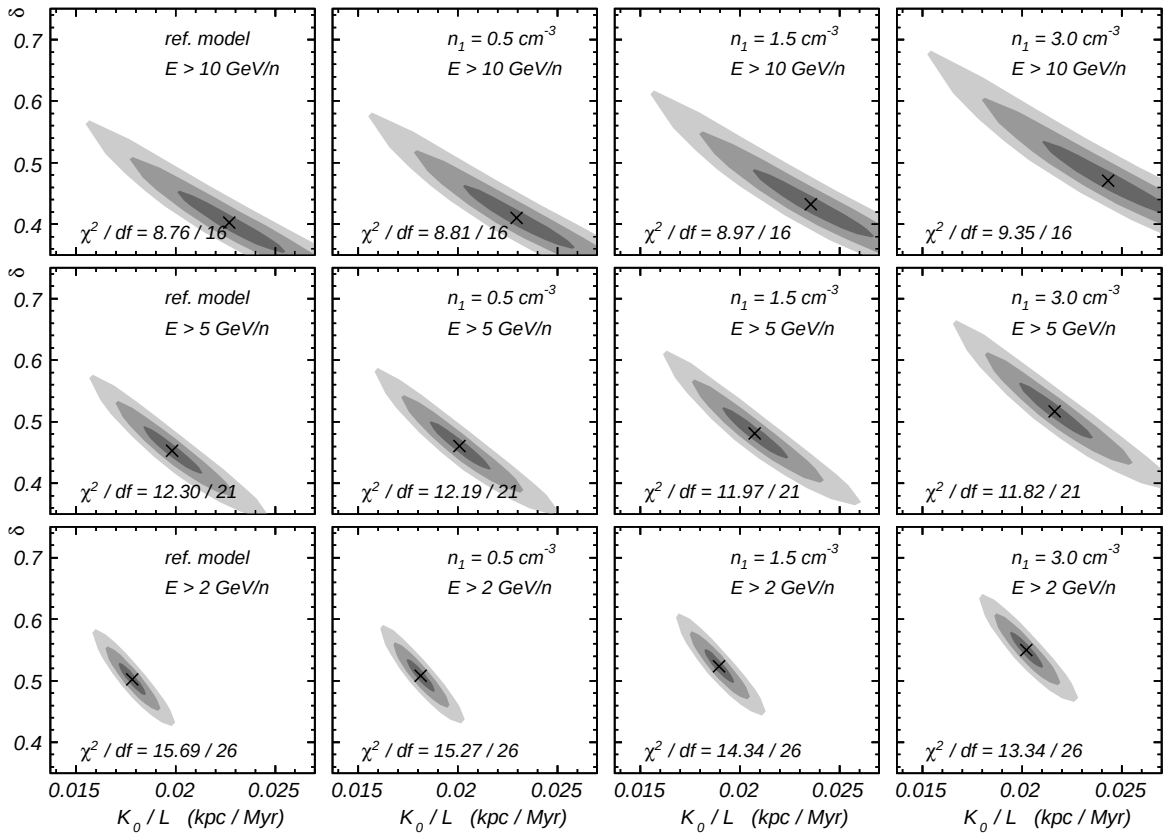

Fig. 4. Fit results for the parameters δ and K_0/L of our models with fragmentation in type I/a SNRs. Results are shown for $E_{\rm min} = 2$, 5 and 10 GeV nucleon^{-1} (top to bottom), for the *reference model* and for the SNR models I/a # 1, # 2 and # 3 (left to right) of Table 2. The shaded areas represent the 1-, 2- and 3-σ contour limits. The markers "×" indicate the best-fit parameters for each configuration; the χ^2/df ratio is reported in each panel.

component arising from ISM collisions (dashed line) and the source component coming from hadronic interactions in SNRs (dotted line). The SNR model is the I/a #3 of Table 2. Note that also the Carbon flux contains a small amount of secondary fragments ($\lesssim 5\%$), produced both in ISM and SNRs. The B/C ratio is also plotted for the *reference model* (dashed line) under the same propagation parameter setting, *i.e.* when hadronic interactions in SNRs are turned off. The effect of including secondary production in the sources translates into a slight increase at 100 GeV nucleon^{-1}, while it reaches a factor 2.5 at 1 TeV nucleon^{-1} and one order of magnitude at 10 TeV nucleon^{-1}.

From the B/C ratio data, we have determined the parameters K_0/L and δ for the type I/a SNR models of Table 2. We have performed a χ^2 analysis using our model interfaced with `MINUIT`. The data are fit above a minimal energy of $E_{\rm min} = 10$ GeV nucleon^{-1}, as a compromise between the diffusion–dominated regime and the availability of experimental data. We have also repeated the fits down to lower $E_{\rm min}$ to test the relevance of low energy effects under our model. The results are shown in Fig. 4 for $E_{\rm min} = 2$, 5 and 10 GeV nucleon^{-1} (from top to bottom), for *reference model* and I/a models of Table 2 (left to right). The shaded areas represent the 1–, 2– and 3–σ contour limits of the χ^2. We stress that such parameter uncertainties are those arising from the fits and they are contextual to our models. Due to the complexity of the physics processes involved together with the possible mis-knowledge of several astrophysical inputs, the actual parameter uncertainties may be much larger (Maurin et al., 2010). For instance, the published values on δ vary well from ~ 0.3 to ~ 0.7. The markers describe the best-fit parameters for each configuration. The χ^2 values reported in each panels are divided by the degrees of freedom: $df = 26$, 21 and 16 for the considered energy thresholds. It can be seen from Fig. 4 that the source component has a little effect for model I/a #3 ($n_1 = 0.5\,{\rm cm}^{-3}$). When denser media are considered, the secondary source component flattens the B/C ratio, so that higher values of δ are requested to match the data. This trend is clearly apparent in Fig. 4 (from left to right). Similar conclusions, though weaker, can be drawn for the K_0/L parameter ratio. To first approximation B/C $\propto L/K_0$, so that the presence of a SNR component of Boron requires a higher K_0/L ratio to match the data.

In summary, for the SNR models considered, the fragmentation in SNRs affects the parameter δ of ~ 5–15% (and K_0/L of ~ 2–10%), but these models cannot be discriminated by present data because of the large uncertainties in the data. This n_1–δ degeneracy is apparent by the χ^2/df–values, which are almost insensitive to the SNR properties.

4.5. Re-Acceleration in Core-Collapse SNRs

The amount of re-accelerated CRs depends on the total volume occupied by the SNRs (per unit time) and their explosion rate (per unit volume). The fraction of re-accelerated CRs to the total background CRs can be roughly estimated as $N^{\rm re}/N^{\rm bg} \sim V_{\rm snr}\mathcal{R}_{\rm snr}\tau_{\rm esc}$, where $V_{\rm snr}$ is the SNR volume and $\tau_{\rm esc}$ is the characteristic escape time of CRs in the Galaxy. At few GeV nucleon^{-1},

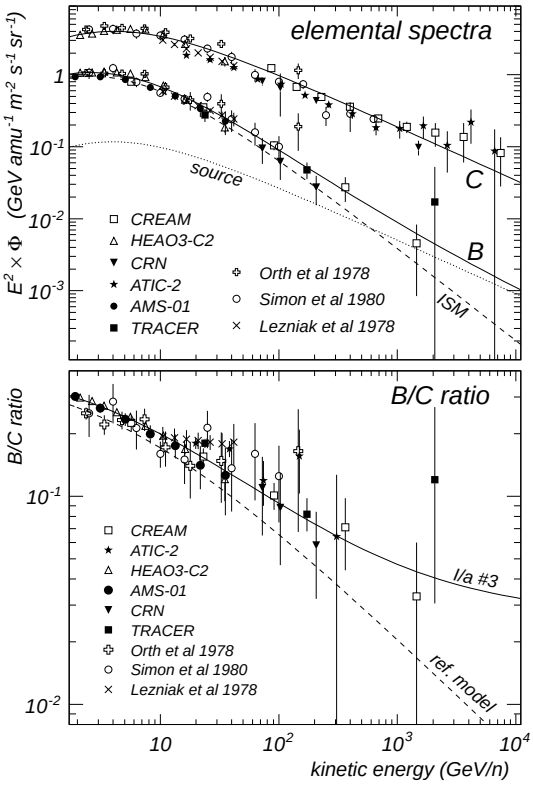

Fig. 3. Top: individual CR spectra of B and C. Solid lines are the model predictions for I/a #3 SNR model of Table 2. Model parameters are as in Table 1 except for δ and K_0/L that are fitted to data. The Boron SNR component (dotted line) and the ISM component (dashed lines) are reported. Bottom: the B/C ratio from the above model (solid line) and when fragmentation in SNR is turned off (dashed line). Data are from HEAO3-C2 (Engelmann et al., 1990), CREAM (Ahn et al., 2009), AMS-01 (Aguilar et al., 2010), TRACER (Obermeier et al., 2011), ATIC-2 (Panov et al., 2007), CRN (Müller et al., 1991), Simon et al. (1980), Lezniak & Webber (1978) and Orth et al. (1978).

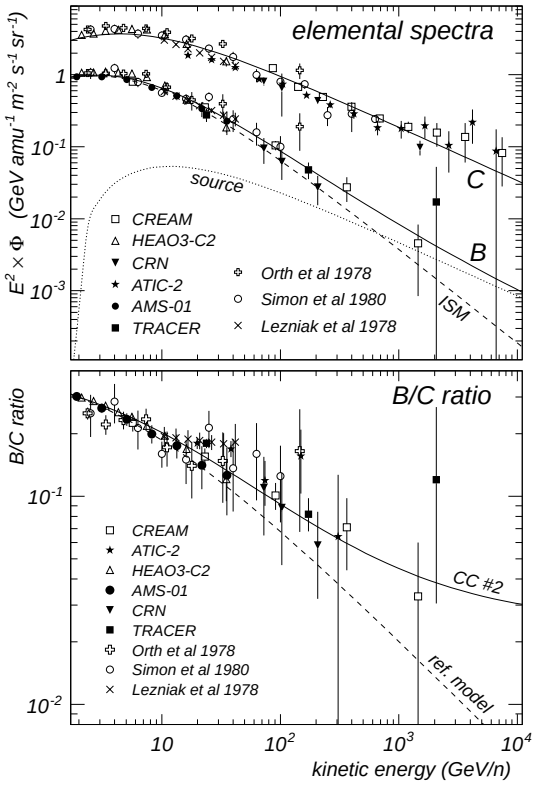

Fig. 5. Top: individual CR spectra of B and C. Solid lines are the model predictions for CC #2 SNR model of Table 2. Model parameters are as in Table 1 except for δ and K_0/L that are fitted to data. The Boron SNR component (dotted line) and the ISM component (dashed lines) are reported. Bottom: the B/C ratio from the above model (solid line) and when re-acceleration is turned off (dashed line). Data as in Fig. 3.

$\tau_{\rm esc} \sim 2hL/K \sim 5\,$Myr. The $V_{\rm snr}$ is mainly determined by its expansion during the ED phase; the SNR reaches a spherical volume $V_{\rm sw} = M_{\rm ej}/(\bar{m}n_1)$, where $\bar{m}$ is the mean mass of the ambient gas. Thus $N^{\rm re}/N^{\rm bg} \propto 1/n_1$, which is an opposite trend with respect to the fragmentation scenario of Sect. §4.4. One can see that for a density $n_1 \sim 1\,{\rm cm}^{-3}$ the re-acceleration gives a small contribution to the total CR flux. On the contrary, for $n_1 \lesssim 0.01\,{\rm cm}^{-3}$, the re-acceleration fraction grows significantly ($\gtrsim$ few percent). However it is also important the subsequent ST phase, where the SNR shock expands adiabatically as $R_{\rm sh}(t) \propto t^{2/5}$, slowing down at the rate $u_1(t) = t^{-3/5}$.

Using the SNR parameters of Table 2, we compute the re-accelerated CR spectra as in Sect. §2.2, using $Q^{\rm reac} = f^{\rm bg}(p)\delta(x)$, where $f^{\rm bg}(p) = \frac{\beta N(p)}{4\pi A p^2}$. Since CRs are already supra-thermal, we assume that all CR particles above $p^{\rm inj}$ are suitable for (re-)undergoing DSA. Note that $N(p)$ is the DHM solution of Eq. 22 which, in turn, is fed by the total DSA spectra. Hence, we solve the DSA and DHM equation systems iteratively. At the first iteration, only the standard injection term is considered (Eq. 12) to compute the interstellar flux N for all CR nuclei. The subsequent iterations make use of the previous DHM solutions, N, to update the terms $Q^{\rm pri}$ and $Q^{\rm reac}$ and to re-compute the total interstellar fluxes. The procedure is iterated until the convergence is reached. At each iteration, the injection constants, Y, are re-adjusted. The resulting CR flux (standard plus re-accelerated) is therefore determined by Eq. 18 and it is fully specified by the source parameters n_1 and $\tau_{\rm snr}$. In practice 5 iterations ensure a stable solution. The effect of re-acceleration is shown in Fig. 5 for the SNR model CC #2 of Table 2. At energies of $\sim 1\,$TeV nucleon^{-1}, the re-accelerated component dominates over the ISM-induced component for secondary nuclei. It should be noted that the sources of re-accelerated CRs may have a complex spatial distribution depending on the SNR spatial profile. In our model we used a uniform distribution, $s(r) \equiv 1$, which does not limit the predicting power of diffusion models as long as the key parameters are regarded as effective quantities tuned to agree with the data (Maurin et al., 2001). However, further elaborations could require more refined descriptions. In Fig. 6 we plot the fit results on the parameters δ and K_0/L for the core-collapse SNR models of Table 2 and for the *reference model*. Compared to the scenario of Sect. §4.4, the results are less trivial to interpret because the background CR flux which is subjected to re-acceleration depends itself on the parameters δ and K_0/L. As consequence of this non-linearity, the K_0/L best-fit values result less sensitive to n_1. The results for δ are qualitatively similar to those of Sect. §4.4, showing an opposite dependence on n_1. For the SNR model CC # 1 ($n_1 = 0.003\,{\rm cm}^{-3}$, left column), the source component dominates the secondary CR flux at $\sim 100\,$GeV nucleon^{-1} so that, at higher energies, the B/C ratio becomes appreciably flat. The effect becomes less significant for higher background densities, *e.g.*, CC # 1 ($n_1 =$

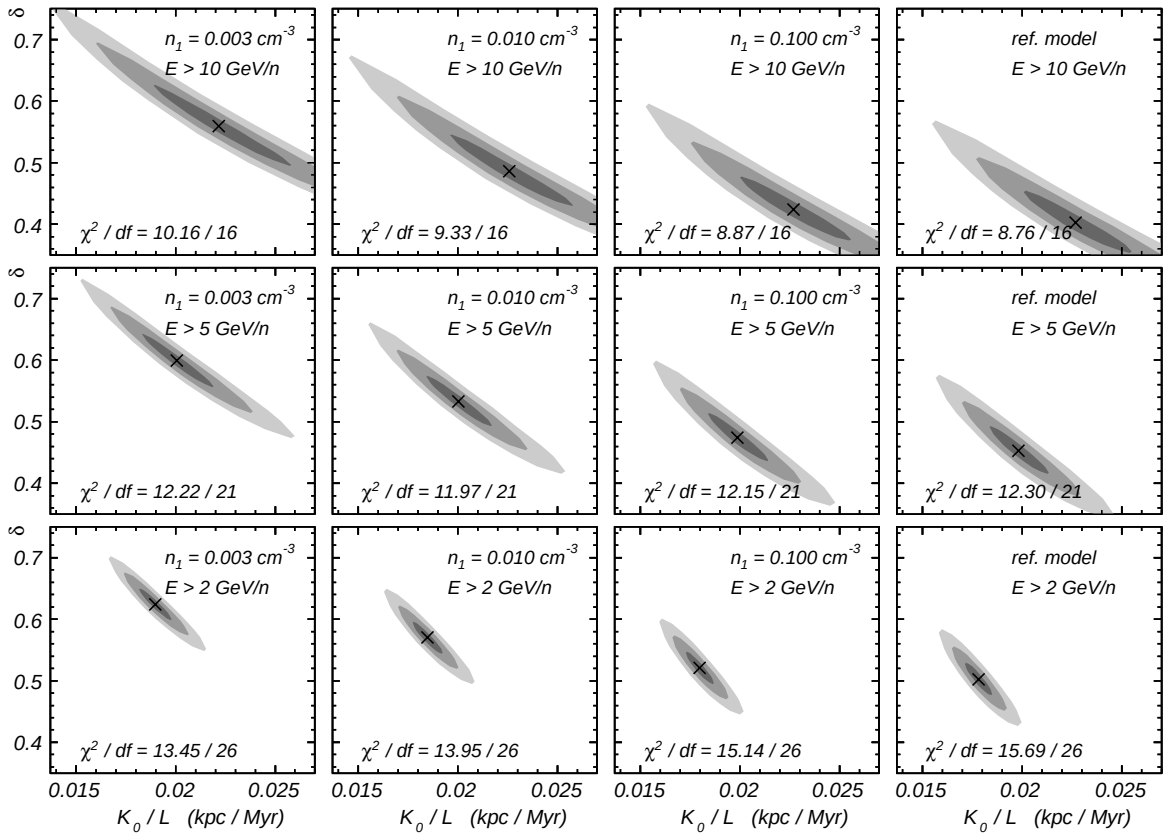

Fig. 6. Fit results for the parameters δ and K_0/L of our models with re-acceleration in core-collapse SNRs. Results are shown for $E_{\rm min} = 2$, 5 and 10 GeV nucleon^{-1} (top to bottom), for the SNR models CC # 1, # 2, # 3 of Table 2 and for the *reference model* (left to right). The shaded areas represent the 1-, 2- and 3-σ contour limits. The markers "×" indicate the best-fit parameters for each configuration; the χ^2/df ratio is reported in each panel.

0.1 cm^{-3}, right column) where the best-fit parameters are close to those arising from the *reference model* fit. As for the scenario of Sect. §4.4, results are limited by the sizable uncertainties in the parameters that preclude quantitative conclusions for $E_{\rm min} = 10$ GeV nucleon^{-1}. Nonetheless, the figure shows clear trends, especially for δ. The χ^2/df values reported in each panels indicates that good fits can be done for all the considered configurations, though they do not vary significantly among the various SNR models.

4.6. Summary and Discussion

Our breakdown into two type I/a and core-collapse SNR scenarios is motivated by the complementary dependence of the two effects on n_1. As seen in Sect. §4.4 and Sect. §4.5, the CR re-acceleration is found to be important for SNRs exploding into rarefied media which are typical of super-bubbles (including our own *local bubble*), while the secondary production in SNRs is relevant for ambient densities similar to those of the regular ISM. Our calculations for the B/C ratio are in substantial agreement with the work of Berezhko et al. (2003) in the cases where the comparison can be made, though they used different approaches for modeling the acceleration as well as for the interstellar propagation. The fit results for the SNR models of Table 2 and for the *reference model* are listed in Table 3.

Figure 7 gives a summary of our findings, showing the best-fit parameters as functions of the SNR circumstellar density. The panel groups (a), (b) and (c) are referred to fits performed at different minimal energies, $E_{\rm min} = 10$, 5, and 2 GeV nucleon^{-1} respectively. For each group, we report δ, K_0/L and χ^2/df as functions of n_1 (from bottom to top, solid lines). The two mechanisms are presented separately: the sub-panels on the left side show the effect of re-acceleration in CC type SNRs, while the right side plots are referred to the secondary production by spallations in type Ia SNRs. The complementarity of the two effects is apparent from the figure. In the region where they overlap, $n_1 \approx 0.5$ cm^{-3}, neither is relevant. The horizontal (dotted) lines indicate the best-fit parameters under the *reference model*. Their dependence on $E_{\rm min}$ resembles that found in Di Bernardo et al. (2010), which also consider diffusive reacceleration models, but we used a different set of data for the parameter determination. As discussed, the *reference model* is insensitive to n_1 or other SNR parameters. The dashed lines indicate the parameter uncertainties (at one σ of CL) arising from the fits.

It is interesting to note the evolution of the best-χ^2 structures when the minimal energy $E_{\rm min}$ is decreased from 10 GeV nucleon^{-1} (Fig. 7a) down to 2 GeV nucleon^{-1} (Fig. 7c). When the low-energy B/C data are included in the fits, the χ^2/df distribution exhibits two minima. In fact the B/C ratio data at low energies favor a slope ($\delta \sim 0.6$) which is rather steeper than that observed in high energy data ($\delta \sim 0.4$): these two regimes are matched by models of SNRs that emit secondary nuclei. In some works, *e.g.* Trotta et al. (2011), it is found that the secondary-to-primary ratios can be reproduced well at all energies using $\delta = 1/3$ and a strong diffusive reacceleration (the interstellar Alfvénic speed is of the order of ~ 30 km s^{-1}). However this de-

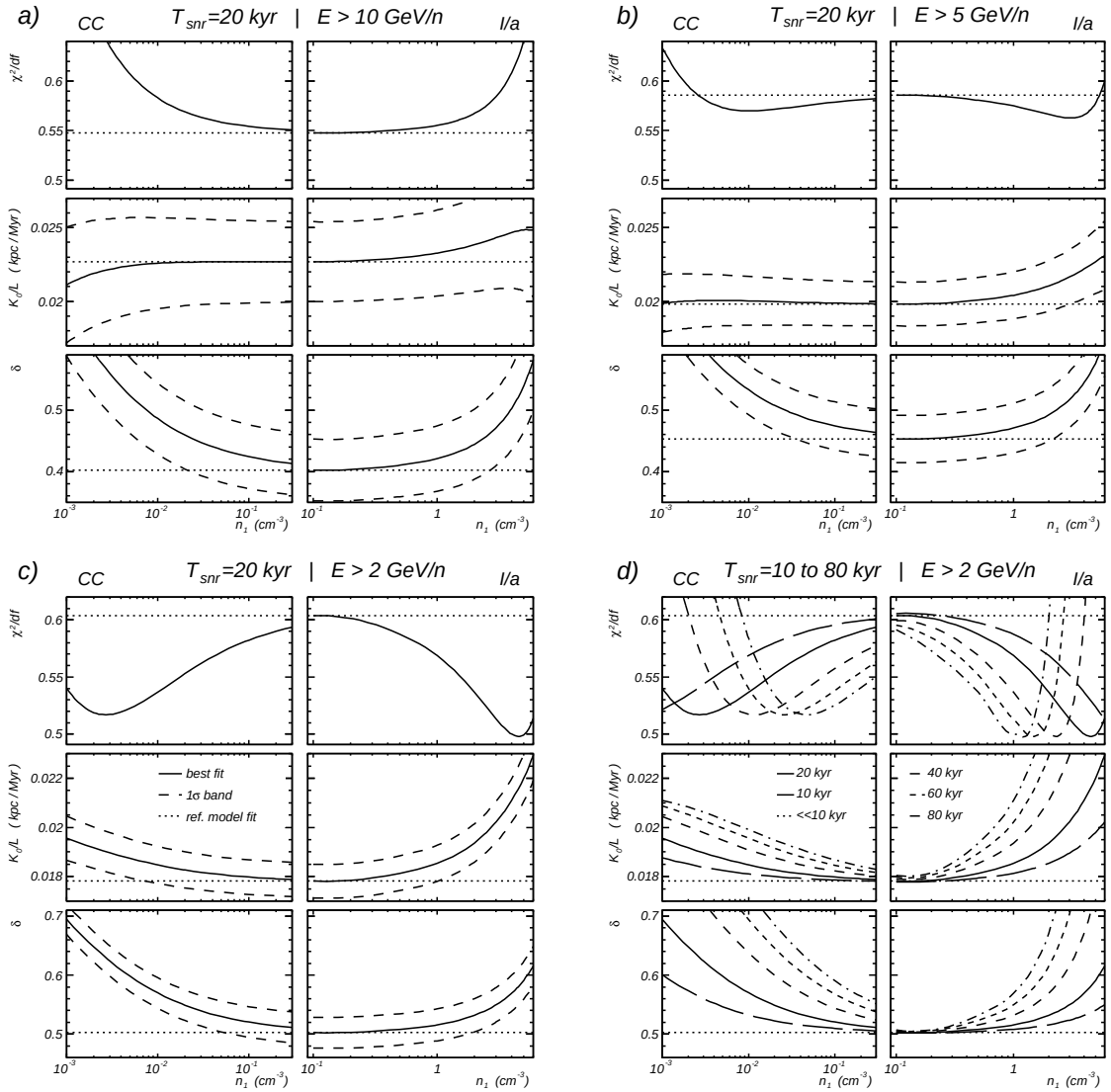

Fig. 7. Best-fit parameters δ and K_0/L and the corresponding χ^2/df as function of n_1 (solid lines) for models with re-acceleration in core-collapse SNRs (*CC*, left sub-panels) and with hadronic interactions in type I/a SNRs (*I/a*, right sub-panels). The panel groups (a), (b) and (c) show the fit results for data at $E_{\rm min} = 1$, 10, 5 and 2 GeV nucleon^{-1}, respectively, for $\tau_{\rm snr} = 20$ kyr. Panel (d) shows the results for $\tau_{snr} = 10$, 20, 40, 60 and 80 kyr in the case of $E_{\rm min} = 2$ GeV nucleon^{-1}. The horizontal dotted lines indicate the *reference model* parameters.

scription cannot be satisfactorily conciliated with the use of pure power-law functions for the CR sources. On the other hand, the trends we observe suggest a possible role of SNR-fragmentation or re-acceleration in conciliating the low-energy B/C data with those at higher energies under a pure diffusion picture.

As we stressed, the physical effects discussed in this work should be tested at high energies, where most of the complexity of the low-energy CR propagation can be neglected. Due to the scarcity of CR data above 10 GeV nucleon^{-1}, the parameter constraints reported in Fig. 7a do not allow any firm discrimination among the different SNR models. However the main trends are apparent. On the propagation side, all the non-standard scenarios point toward larger values for δ, which is in some tensions with expectations for the interstellar turbulence (Strong et al., 2007) and with indications arising from CR anisotropy studies (Ptuskin et al., 2006). On the acceleration side, large values of δ reduce the source spectral index closer to the value $\nu = 2$, which is favored by the DSA theory for strong shocks.

In all these scenarios the acceleration ceases at $\tau_{\rm snr} = 20$ kyr, which may not be the case given their different SNR evolutionary properties. For instance, since the ST phase duration scales as $n_1^{-4/7}$ (Truelove & McKee, 1999), one may expect that core-collapse SNRs have larger $\tau_{\rm snr}$ than type I/a SNRs. However the parameter $\tau_{\rm snr}$ represents the time for which the SNR is active as CR factory and it can be highly non trivial to be estimated. Thus, in Fig. 7d, we give the fit results for different values of τ_{snr} from 10 kyr to 80 kyr ($E_{\rm min} = 2$ GeV nucleon^{-1}). The effect of using different $\tau_{\rm snr}$ is clear. Longer is the time for which the SNR is active, more are the fragments produced in its interior. In practice the secondary CRs production in type I/a SNRs is characterized by product $n_1\tau_{\rm snr}$. For re-acceleration, a larger lifetime allows the SNR to occupy larger volumes. To first approximation the intensity of re-accelerated nuclei increases as $\sim \tau_{\rm snr}/n_1$. As shown in the figure, for larger values of $\tau_{\rm snr}$, the re-acceleration effect becomes important also for relatively high density media.

Table 3. Summary of the fit results to the propagation parameters. See the text in Sect. §4.6.

Fit	$E > 2$ GeV/n			$E > 5$ GeV/n			$E > 10$ GeV/n		
Model	δ	K_0/L (kpc/Myr)	χ^2/dof	δ	K_0/L (kpc/Myr)	χ^2/dof	δ	K_0/L (kpc/Myr)	χ^2/dof
Ref. Model	0.50 ± 0.03	0.01781 ± 0.00069	15.69/26	0.45 ± 0.04	0.01982 ± 0.00149	12.30/21	0.40 ± 0.05	0.02270 ± 0.00270	8.76/16
SNR I/a # 1	0.51 ± 0.03	0.01813 ± 0.00071	15.27/26	0.46 ± 0.04	0.02008 ± 0.00153	12.19/21	0.41 ± 0.05	0.02296 ± 0.00280	8.81/16
SNR I/a # 2	0.52 ± 0.03	0.01895 ± 0.00075	14.34/26	0.48 ± 0.04	0.02073 ± 0.00165	11.97/21	0.43 ± 0.06	0.02357 ± 0.00304	8.97/16
SNR I/a # 3	0.55 ± 0.03	0.02022 ± 0.00083	13.34/26	0.52 ± 0.05	0.02164 ± 0.00185	11.82/21	0.47 ± 0.06	0.02432 ± 0.00346	9.35/16
SNR CC # 1	0.62 ± 0.03	0.01897 ± 0.00082	13.45/26	0.60 ± 0.04	0.02005 ± 0.00179	12.22/21	0.56 ± 0.07	0.02217 ± 0.00343	10.16/16
SNR CC # 2	0.57 ± 0.03	0.01847 ± 0.00076	13.95/26	0.53 ± 0.04	0.02003 ± 0.00165	11.97/21	0.49 ± 0.06	0.02258 ± 0.00308	9.33/16
SNR CC # 3	0.52 ± 0.03	0.01798 ± 0.00070	15.14/26	0.47 ± 0.04	0.01988 ± 0.00152	12.15/21	0.42 ± 0.05	0.02269 ± 0.00279	8.87/16

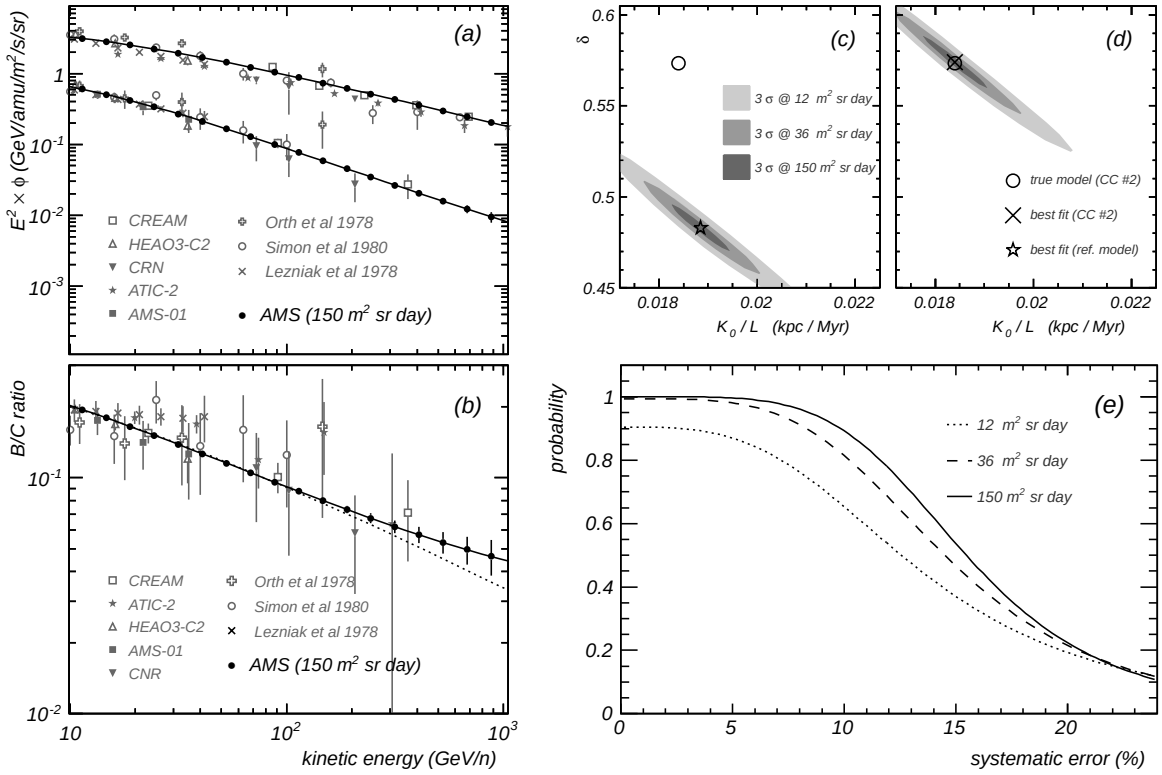

Fig. 8. AMS-02 mock data for the elemental fluxes ϕ_B and ϕ_C (a) and their ratio (b), using the input model CC # 2 of Table 2 and assuming a detector exposure factor F= 150 m^2 sr day. The error bars are only statistics. The constraints to the transport parameters provided by the AMS-02 mock data are reported by the 3-σ contour levels for exposure factors of $F = 12$, 36 and 150 m^2 sr day in (c) and (d). The data are fitted within the reference model (star in panel c and dotted line in panel b) and within the model CC # 2 (cross in panel d and solid line in panel b). The AMS-02 discrimination probability between the two models as a function of the systematic error in the measurement is shown in (d) for F= 12, 36 and 150 m^2 sr day. The systematic errors are assumed to be energy-independent.

5. The Projected AMS-02 Sensitivity

We switch now to some estimations for the AMS experiment[1], that is devoted to direct measurements of galactic CRs in a wide range of energy. Prime goals of the AMS project are the direct search of anti-nuclei and the indirect search of dark matter particles. The first version of the experiment, AMS-01, operated in a test flight on June 1998. The final version of experiment, AMS-02, was successfully installed in the *International Space Station* on May 2011 and will be active for at least 10 years. AMS-02 is able to identify CR elements from $Z = 1$ to $Z = 26$ and determine their energy spectra from ~ 0.5 GeV to ~ 1 TeV per nucleon with unprecedented accuracy. We estimate the AMS-02 capabilities in determining the CR propagation properties for the considered scenarios.

5.1. Projected data

The AMS-02 sensitivity to CR nuclei measurements is studied by the generation of *mock* data for a given input model. The number of j–type particles recorded by AMS-02 at the kinetic energies between E_1 and E_2 is given by:

$$\Delta N_j = \int_{E_1}^{E_2} \phi_j(E) \cdot \mathcal{E}_j \cdot \mathcal{G}_j \cdot \mathcal{T}_j \cdot dE \,, \qquad (27)$$

where ϕ_j is the input spectrum, $\mathcal{G}_j$ is the detector geometric factor, $\mathcal{E}_j$ is the detection efficiency and $\mathcal{T}_j$ is the exposure time. All

[1] http://www.ams02.org

these quantities are in general energy-dependent and particle-dependent. Relevant for our estimates is the exposure factor $\mathcal{F} \equiv \mathcal{E}\mathcal{G}\mathcal{T}$ that we take as energy and particle independent. We consider the cases of $\mathcal{F} = 12$, 36 and 150 $\mathrm{m^2\,sr\,day}$. For values of, *e.g.*, $\mathcal{G} = 0.45\,\mathrm{m^2\,sr}$ and $\mathcal{E} = 90\%$, our choices correspond to 1 month, 3 month and 1 year of time exposures, respectively, We adopt a log-energy binning using 9 bins per decade between 10 GeV and 1 TeV per nucleon. The AMS-02 mock data for the B and C fluxes and their ratio are shown in Fig. 8a and 8b. The CR fluxes, ϕ_B and ϕ_C, are calculated using the SNR model CC # 2 (Table 2) as input model. This "true" model is characterized by SNR parameters $n_1 = 0.01\,\mathrm{cm^{-3}}$ and $\tau_{\rm snr} = 20\,\mathrm{kyr}$, and transport parameters $K_0/L = 0.01847\,\mathrm{kpc\,Myr^{-1}}$ and $\delta = 0.57$. From Eq. 27, we compute the statistical error of each B/C data point as $1/\sqrt{\Delta N_B} + 1/\sqrt{\Delta N_C}$. Nonetheless, CR measurements are also affected by systematic errors, that become more and more important as the precision increases with the collected statistics.

5.2. Discrimination Power

We fit the B/C ratio mock data leaving K_0/L and δ as free parameters. These parameters are determined within the *reference model* (re-acceleration off) and within the "true" re-acceleration model CC # 2 of Table 2. As shown in Fig. 8b, both the models can be tuned to reproduce the AMS-02 mock data, but they exhibit different functional shapes and deviate at high energies. The contour plots in panels (c) and (d) correspond to the best-fit parameters of the two models. Contour levels are shown for 3-σ uncertainty corresponding to the three exposure factors $\mathcal{F}$. As expected, the re-acceleration model fit (d) returns back the correct parameters, while the *reference model* fit (c) misestimates parameters due to our inaccurate assumptions on the source properties. In fact, when the *reference model* is forced to describe the data, the spectral distortion induced by the re-acceleration is mimicked by the use of a lower value for δ. Given the precision of the AMS-02 data, this represents the dominant "error" in the parameter determination. As apparent from the figure, the AMS-02 data set tight constraints to the propagation parameters. For instance, δ is determined with a precision better than $\lesssim 10\%$ within 3–σ of uncertainty. The δ–n_1 degeneracy may be lifted as done in Castellina & Donato (2005), *i.e.*, by a statistical test to discriminate the two fits. As long as only statistical errors are considered, we find that the discrimination between the two scenarios is always possible for the three considered exposures at 90 % of CL. The effect of systematic errors in the data is shown in Fig. 8e, where we plot the AMS-02 discrimination probability versus the relative systematic error. Our calculation assumes constant systematic errors (added in quadrature to the statistical ones), but these considerations also hold for energy-dependent systematic errors if their energy rise is less pronounced that than the statistical errors. The solid, dashed and dotted lines represent the cases of $\mathcal{F} = 12$, 36 and 150 $\mathrm{m^2\,sr\,day}$ respectively. In order to achieve a discrimination of 90% CL, the systematic error has to be lower than $\sim 4\%$, 8% and 10% for the three considered exposures. A 95% CL requirement also needs that $\mathcal{F}$ to be larger than $12\,\mathrm{m^2\,sr\,day}$. We consider these requirements as reasonable for AMS-02, because the measurements of elemental ratios are only mildly sensitive to systematic errors.

Similar conclusion can be drawn for models with fragmentation in SNRs. In this case we have explored a large region of the parameter space n_1–δ, with $\delta = 0.3$–0.8 and $n_1 = 0$–$5\,\mathrm{cm^{-3}}$. Our estimate is carried on as follows. For each $\{n_1, \delta\}$ parameter combination, we determine K_0/L from fits to the existing B/C ratio data. Then we define the true model using $\{n_1, \tau_{\rm snr}\}$ as source parameters and $\{\delta, K_0/L\}$ as transport parameters. From the true model, we generate the AMS-02 mock data for a given exposure factor, $\mathcal{F}$, and 5 % of systematic error. Thus, we re-fit the mock B/C ratio, leaving K_0/L and δ as free parameters, within the *reference model* and within the true SNR scenario (fragmentation specified by n_1). Finally, we estimate the AMS-02 discrimination probability for the two models. The shaded areas of Fig. 9 indicate the parameter region where the AMS-02 discrimination succeeds at 95% CL for $\mathcal{F} = 12$, 36 and 150 $\mathrm{m^2\,sr\,day}$. The figure shows that AMS-02 is sensitive to a large region of the parameter space, except for small n_1 values (small secondary SNR component) and/or small δ values (hard ISM component), when the intensity of the secondary source component is too weak to induce appreciable biases in the propagation parameters. This is also the case of Kolmogorov-like diffusion ($\delta = 1/3$) which, however, is disfavored by our analysis of the real data. These considerations can be much strengthened if one considers the independent constraints that may be brought by other AMS-02 data such as, for example, the ratios $\overline{\mathrm{p}}$/p, Li/C, F/Ne or Ti/Fe. In summary, our estimates show that AMS-02 has good performances in determining the CR transport parameters, providing tight constraints and considerable progress in understanding the CR acceleration and propagation processes.

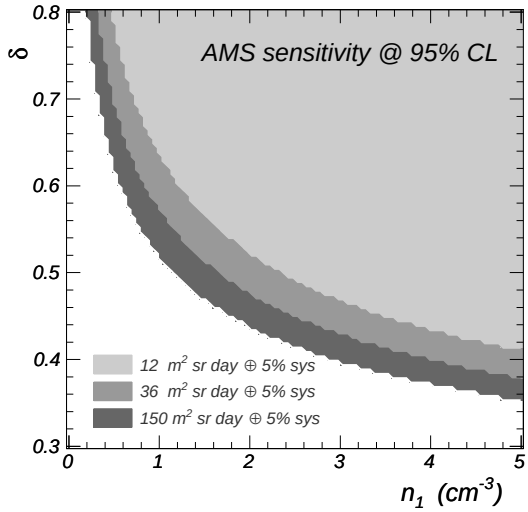

Fig. 9. AMS-02 discrimination power for models with secondary production in SNRs. Each point in the (n_1, δ)–plane represents an input model with fragmentation inside SNRs with $\tau_{\rm snr} = 20$ kyr. The parameter K_0/L is taken to match the existing B/C ratio data. The shaded areas cover the parameter region where AMS-02 is sensitive at 95% CL for the exposure $\mathcal{F} = 12$, 36 and 150 $\mathrm{m^2\,sr\,day}$. The systematic errors are assumed to be 5% of the measured B/C and constant in energy.

6. Conclusions

We have studied the CR propagation physics under the scenarios where secondary nuclei can be produced or re-accelerated from galactic sources. We have considered the processes of secondary productions inside SNRs and re-acceleration of background CRs in strong shocks. The two mechanisms are complementary to each other and depend on the properties of the local ISM around the expanding remnants. The secondary production in SNRs is significant for dense background media, $n_1 \gtrsim 1\,\mathrm{cm^{-3}}$, while the amount of re-accelerated CRs is relevant for SNRs expanding

into rarefied media, $n_1 \lesssim 0.1\,\mathrm{cm}^{-3}$. Consequence of both mechanisms is a slight flattening of the secondary-to-primary ratios at energies above $\sim 100\,\mathrm{GeV\,nucleon}^{-1}$. For B/C ratio the increse may be a factor of few at 1 TeV nucleon^{-1} and reach an order of magnitude at 10 TeV nucleon^{-1}. Modeling these effects introduce an additional degeneracy between the source and the transport parameters. The diffusion coefficient index δ, determined from the B/C ratio measurements above $\sim 10\,\mathrm{GeV\,nucleon}^{-1}$, turns out to be mis-estimated by a factor of $\gtrsim 15\,\%$ if the underlying model does not account for the hadronic production in SNRs with $n_1 \gtrsim 2\,\mathrm{cm}^{-3}$ or for re-acceleration with $n_1 \lesssim 0.02\,\mathrm{cm}^{-3}$. Nonetheless, the current uncertainty in δ is much larger as the existing data suffer for lack of precision at $E > 10\,\mathrm{GeV\,nucleon}^{-1}$. We have shown that this degeneracy may be at least partially broken with data collected by high precision experiments such as AMS-02. Would propagation in the Galaxy be described by a Kolmogorov spectrum (δ=0.33), it will not be mis-understood with possible source effects described in this work, because they are expected to give small distortions to the hard B/C ratio. On the other side, we have shown that for $\delta \sim 0.4 - 0.8$ an AMS-02 like experiment will be able to discriminate pure propagation trends from a source contribution. Data around TeV nucleon^{-1} energies will be clue at this aim. Systematic errors contained to a $\sim$ 10% level will not prevent a clear discrimination between *reference model* propagated CRs and a non negligible source production.

Data from single elements and antiprotons will contribute to identify the possible source effects studied in this research. Further inspections, including the revision of the role of convection and diffusive reacceleration, require more data at high energies. They may be released soon by a number of active experiments. The long duration balloon projects CREAM and TRACER, and the space missions AMS-02 and PAMELA are currently exploiting unprecedented sensitivities and energy ranges. Their data will provide valuable pieces of information about the CR acceleration and propagation physics.

Acknowledgements. We warmly thank B. Bertucci and P. D. Serpico for a careful reading of the manuscript.

References

Aguilar, M., et al., 2010, ApJ, 724, 329–340 (AMS-01)
Ahlers, M., Mertsch, P., & Sarkar, S., 2009, PRD, 80, 123017
Ahn, H., S., et al., 2009, ApJ, 707, 593–603 (CREAM)
Ave, M., Boyle, P. J., Gahbauer, F., Höppner, C., Hörandel, J., R., Ichimura, M., Müller, D. & Romero-Wolf, A., 2008, ApJ, 678, 262–273 (TRACER)
Berezhko, E. G., Ksenofontov, L. T., Ptuskin, V. S., Zirakashvili, V. N. & Völk, H. J., 2003, A&A, 410, 189–198
Blasi, P., 2009, PRL, 103, 051104
Blasi, P., & Serpico, P. D., 2009, PRL, 103, 081013
Castellina, A., & Donato, F., 2005, A.Ph, 1–2, 146–159
Di Bernardo, G., Evoli, C., Gaggero, D., Grasso, D., & Maccione, L., 2010, A.Ph, 34-5, 274–283
Drury, L. O'C., 1983, Rep. Prog. Phys., 46, 973–1027
Engelmann, J. J., et al., 1990, A&A, 233, 96–111 (HEAO3-C2)
Ferrando, P., Webber, W. R., Goret, P., Kish, J. C., Schrier, D. A., Soutol, A. & Testard, O., 1988, PRL, 37-4, 1490–1501
Gleeson, L. J., & Axford, W. I 1968, ApJ, 154, 1011
Grenier, I. A., 2000, A&A, 364, L93–L96
Juliusson, E., et al.1974, ApJ, 191, 331
Kachelrieß, M., Ostapchenko, S.,& Tomás, R., 2011, ApJ, 733, 119
Lezniak, J. A., & Webber, W. R., 1978, ApJ, 223, 676–696
Maurin, D., Putze, A., & Derome, L., 2010, A&A, 516, 67
Maurin, D., Donato, F., Taillet, R., & Salati, P., 2001, ApJ, 555, 585
Mertsch, P., & Sarkar, S., 2009, PRL, 103, 081104
Morlino, G., 2011, MNRAS., 412, 2333–2344
Müller, D., Swordy, S. P., Meyer, P., L'Heureux, J. & Grunsfeld, J. M., 1991, ApJ, 374, 356–366 (CRN)
Obermeier, A., Ave, M., Boyle, P. J., Höppner, C., Hörandel, J., R., & Müller, D., 2011, ApJ, 742, 14 (TRACER)
Orth, C. D., et al., 1978, ApJ, 226, 1147–1161
Panov, A., D., et al., 2009, Bull. Russian Acad. Sci., 73(5), 602–605 (ATIC)
Panov, A. D, et al., 2007, Proc. of 30th ICRC (Mérida), 2, 3 (ATIC)
Ptuskin, V., Zirakashvili, V. & Seo, E. S., 2010, ApJ, 718, 31–36
Ptuskin, V., Jones, F. C., Seo, E. S., & Sina, R., 2006, Adv. Sp. Res., 37, 1909–1912
Silberberg, R., Tsao, C. H. & Barghouty, A. F., 1998, ApJ, 501, 911–919
Simon, M, et al., 1980, ApJ, 239, 712–724
Strong, A. W., Moskalenko, I. V., & Ptuskin, V. S., 2007, Ann. Rev. Nucl. & Part. Sci., 57, 285–327
Swordy, S. P., Müller, D., Meyer, P., L'Heureux, J. & Grunsfeld, J. M., 1990, ApJ, 349, 625–633 (CRN)
Taillet, R., & Maurin, D., 2003, A&A, 402, 971–983
Trotta, R., Jóhannesson, G., Moskalenko, I. V., Porter, T. A., Ruiz de Austri, R. & Strong, A. W., 2011, ApJ, 729, 106–122
Truelove, J. K. & McKee, C. F., 1999, ApJ, 120, 299–326
Wandel, A., Eichler, D., Letaw, J. R., Silberberg, R. & Tsao, C. H., 1987, ApJ, 316, 676–690